

Effects of nitrogenation on single-walled carbon nanotubes within density functional theory

San Hua Lim,^{1,2} Ruijiang Li,¹ Wei Ji,² and Jianyi Lin^{1,2,*}

¹*Applied Catalysis, Institute of Chemical and Engineering Sciences, Singapore 627833, Singapore*

²*Department of Physics, National University of Singapore, Singapore 119260, Singapore*

(Received 9 January 2007; revised manuscript received 22 June 2007; published 7 November 2007)

The effects of nitrogenation on single-walled carbon nanotubes are investigated within the *ab initio* density functional theory. Four different types of nitrogenation have been considered: (i) direct substitution of nitrogen atoms, (ii) substitution with a formation of vacancy (pyridinelike doping), (iii) exohedral chemisorption of N adatoms, and (iv) sidewall covalent -NH₂ functionalization. Structural deformations, electronic band structures, density of states, and ionization potential energies are calculated and compared among the different types of nitrogenated nanotubes. Magnetism is observed for chemisorbed single-walled carbon nanotubes (SWNTs) with magnetic moment of 0.7 μ_B . In addition, the relaxed structures of SWNTs with two neighboring chemisorbed N adatoms are generally more complex than those of singly chemisorbed N adatom. The barrier energies needed to coalesce two N adatoms chemisorbed on SWNTs to form a free N₂ molecule are higher than those for a graphene sheet.

DOI: 10.1103/PhysRevB.76.195406

PACS number(s): 81.07.De, 71.15.Mb

I. INTRODUCTION

Single-walled carbon nanotubes (SWNTs) are seamlessly rolled-up graphene sheets of carbon and they can be metallic or semiconducting, depending greatly on their tubular diameter and chirality.¹ Thus, it is difficult to synthesize SWNTs with uniform chirality and electronic properties. To overcome this difficulty, dopants and defects can be introduced to alter the electronic properties of SWNTs. The creation of new energy levels in the band gap with associated electronic states is an important step to make electronic devices.

The intercalation of alkali metals and halogens into SWNT bundles has been utilized to modify the electronic properties.² B and/or N atoms are also good choice of dopants because they have roughly the same atomic radius as C atoms and possess one electron less/more than C, respectively. Nitrogen doping is particularly attractive because the extra electrons from the nitrogen dopants are expected to make semiconducting nanotubes metallic. Various approaches have been made to incorporate nitrogen atoms into carbon nanotubes, including magnetron sputtering,³ pyrolysis of nitrogen-rich organic chemicals,⁴ and arc discharge in nitrogen atmosphere.⁵ However, most of the syntheses yield nitrogen-doped multiwalled carbon nanotubes with bamboo-shaped morphology. Recently, Villalpando-Paez *et al.*⁶ reported the synthesis of nitrogen-doped SWNT bundles via an aerosol-assisted chemical vapor deposition (CVD) method, but the doping concentration is unknown. It has been suggested that the nitrogen dopants are substituted into the carbon network with and without vacancy formation. On the other hand, nitrogenation of pristine carbon nanotubes (CNTs) has also been conducted using ammonia or nitrogen glow discharge,^{7,8} ball milling in ammonia atmosphere,⁹ and N ion implantation¹⁰ methods. These methods exohedrally nitrogenate the sidewalls of CNT with -NH₂ functional groups and chemisorbed N adatoms. In addition, the presence of nitrogen impurities in π -conjugated systems^{11,12} can alter its magnetic properties. Ma *et al.*¹² showed that the chemisorption of a N adatom on a graphite surface possessed a magnetic moment of 0.6 μ_B .

Previously, we had experimentally studied the electronic and optical properties of nitrogen-doped multiwalled carbon nanotubes.⁴ We noted that nitrogen dopants enriched the π electrons, lowered the work function, and consequently enhanced its ultrafast saturable absorption. In this paper, we have furthered our understanding of nitrogenated carbon nanotubes by carrying out a theoretical investigation on its atomic deformation, electronic structures, molecular orbital, ionization potential (IP) energies, spin polarization, and structural stability of chemisorption process.

II. COMPUTATIONAL METHOD

The electronic properties of nitrogenated SWNTs were studied using first-principles density functional theory, DMOL³ code, available from Accelrys Inc.¹³ Each electronic wave function is expanded in a localized atom-centered basis set with each basis function defined numerically on a dense radial grid. For supercell geometries, spin-restricted calculations were carried out with a double numeric polarized basis set available and the atomic cutoff set at 4.5 Å, along with gradient-corrected Perdew-Burke-Ernzerhof functional.¹⁴ Scalar relativistic effects¹⁵ were included via a local pseudopotential for all-electron calculations. Five and eight Monkhorst-Pack *k* points¹⁶ were used for the Brillouin zone integration along the axes of (10,0) and (5,5) nanotubes, respectively. Geometry optimizations were performed with the Broyden-Fletcher-Goldfarb-Shanno (BFGS) algorithm with convergence criterion of 10⁻³ a.u. on gradient and displacement and 10⁻⁵ a.u. on the total energy and electron density. A hexagonal lattice was used to simulate the single-walled nanotubes, with a wall-to-wall distance of at least 10 Å, sufficient to avoid in-plane interactions between nanotubes in adjacent unit cells. The Fermi levels of the spin-restricted band structures and density of states (DOS) of (10,0) nanotubes were reset at the 0 eV position. For DMOL³ code, the molecular orbital of periodic systems was computed using only the Γ point. The isodensity surfaces of the highest occupied molecular orbital (HOMO) of Figs. 1 and 2 were

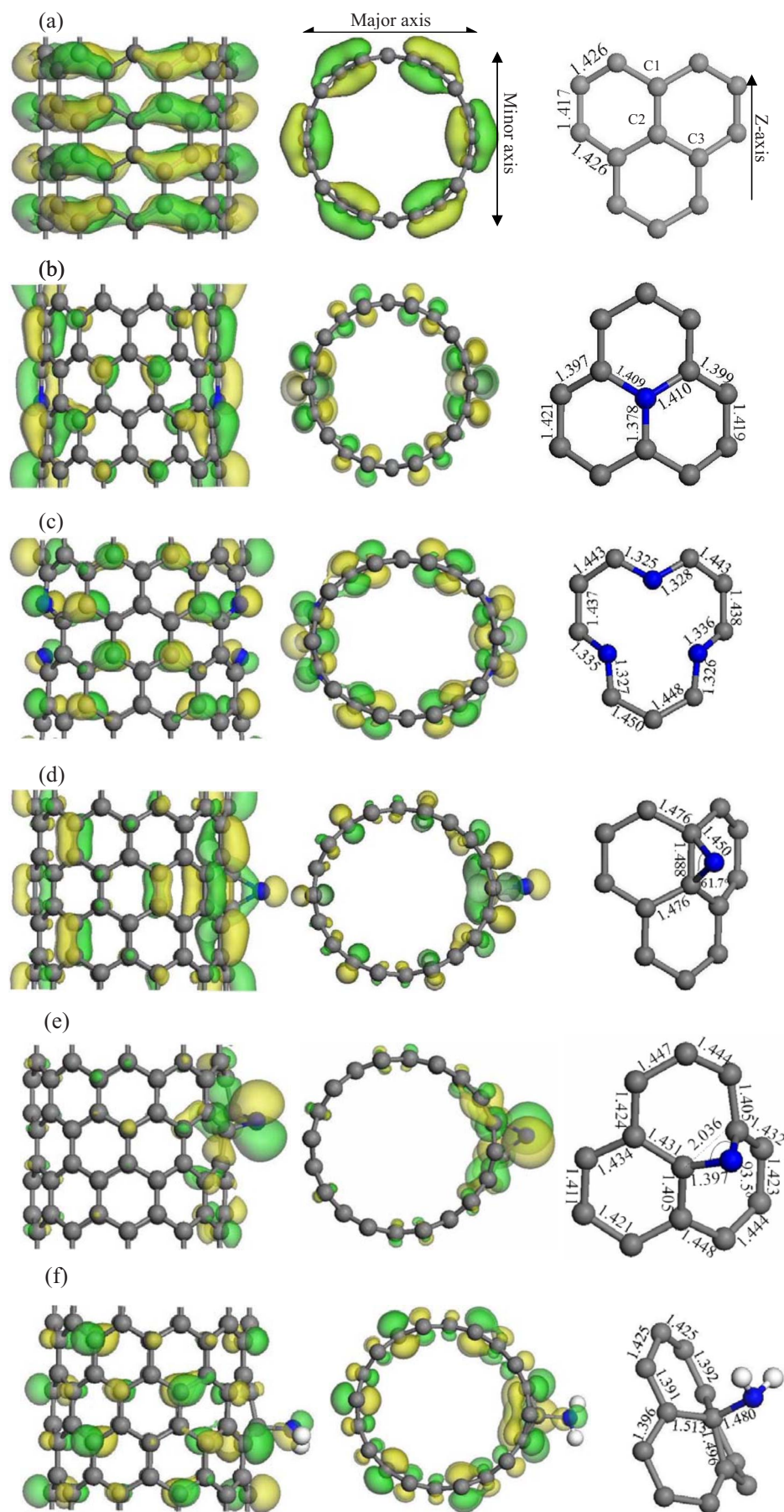


FIG. 1. (Color online) (a) Geometrically optimized structures, HOMO, and bond lengths (in Å) of a pure zigzag (10,0) nanotube. (b) Direct substitution of two nitrogen atoms into the carbon framework without the formation of vacancies. Here, the two N substitution atoms in $C_{78}N_2$ are in the opposite positions. (c) N substitution into the carbon framework with the formation of vacancy: pyridinelike doping ($C_{72}N_6$) with two vacancies formed in opposite positions. (d) Chemisorption of a N adatom in parallel position. (e) Chemisorption of a N adatom in perpendicular position. (f) $-NH_2$ functionalization. Gray ball denotes C atom, blue ball denotes N atom, and white ball denotes H atom. A fragment of the supercell is taken out to elucidate the bond lengths at the vicinity of the N impurities.

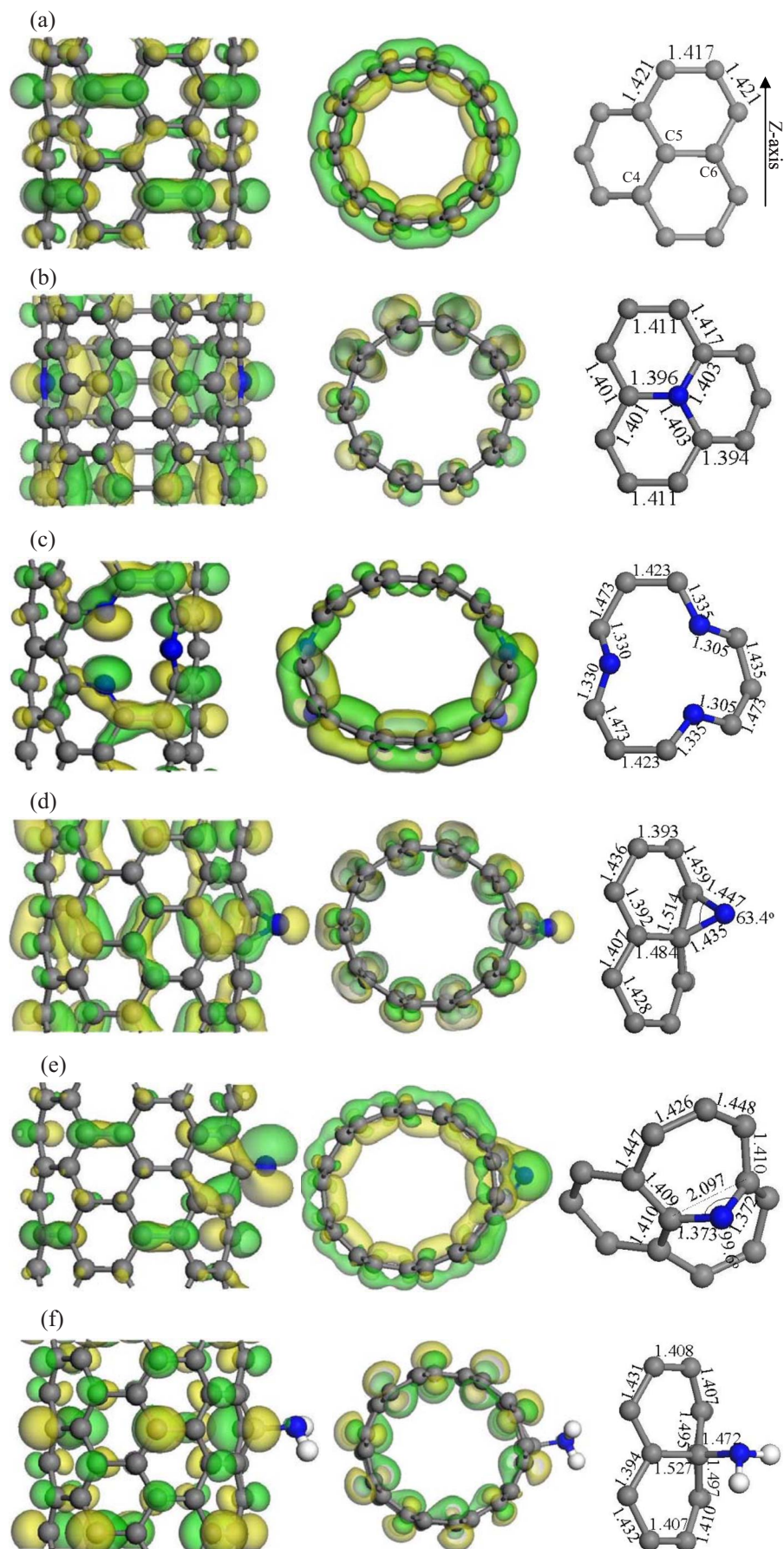


FIG. 2. (Color online) (a) Geometrically optimized structures, HOMO, and bond lengths (in Å) of a pure armchair (5,5) nanotube. (b) Direct substitution of two nitrogen atoms into the carbon framework without the formation of vacancies. Here, the two N substitution atoms in $C_{58}N_2$ are in the opposite positions. (c) N substitution into the carbon framework with the formation of vacancy: pyridinelike doping ($C_{52}N_6$) with two vacancies formed in opposite positions. (d) Chemisorption of a N adatom in parallel position. (e) Chemisorption of a N adatom in perpendicular position. (f) $-NH_2$ functionalization. Gray ball denotes C atom, blue ball denotes N atom, and white ball denotes H atom. A fragment of the supercell is taken out to elucidate the bond lengths at the vicinity of the N impurities.

fixed at $0.02e/a.u.$ ³ A smearing of 0.003 a.u. was applied for all DOS graphs.

Calculations were performed with supercells of zigzag (10,0) [see Fig. 1(a)] and armchair (5,5) SWNTs [see Fig. 2(a)]. The supercell lengths of the zigzag and armchair nanotubes are $a=8.52 \text{ \AA}$ (80 atoms/cell) and $a=7.38 \text{ \AA}$ (60 atoms/cell), respectively, unless otherwise stated. Four types of nitrogenated carbon nanotubes were considered: (i) Direct substitution of nitrogen dopants into the carbon framework without a formation of vacancy [see Figs. 1(b) and 2(b)]. Doping density varies from 0.83 to 5 at. %. (ii) Substitution of nitrogen dopants with vacancy formation by removing a central C atom among three hexagons and replacing the three surrounding C atoms with three N atoms [see Figs. 1(c) and 2(c)]. This pyridinelike structure was proposed by Czerw *et al.*,¹⁷ and this type of N doping is hereinafter termed as pyridinelike doping. Doping density varies from 3.8 to 7.6 at. %. (iii) Exohedral chemisorption of nitrogen adatoms. The chemisorbed N adatoms can be in “parallel” or “perpendicular” positions. The N adatom that bridges over the C-C bond is in a parallel position, while the N adatom that bridges over a broken C-C bond is in a perpendicular position. In Fig. 1(d), for a zigzag nanotube, the N adatom chemisorbed over the C1-C2 bond is in parallel position, while perpendicular position refers to the N adatom bridging the C2-C3 bond which is broken [compare Figs. 1(d) and 1(e)]. For an armchair nanotube, the parallel position refers to the N adatoms above the C4-C5 bond [see Fig. 2(d)], while the perpendicular position is bridged over the C5-C6 bond [in Fig. 2(e), C5-C6 bond is broken]. (iv) Sidewall covalent $-NH_2$ functionalization [see Figs. 1(f) and 2(f)]. Hence, the atomic deformation, bond lengths, molecular orbital, and energetics of nitrogenated SWNTs were presented in Sec. III A. Spin-restricted electronic properties of nitrogenated SWNTs were presented in Sec. III B.

The IP values have been determined for the nitrogenated nanotubes and the results were presented in Sec. III C. The IP is defined as the energy difference between a positively charged system (+1) and the originally neutral system (0). A constant electric field of 1 eV/\AA is applied parallel to the tube axis, whereby field emission is assumed to occur at this order of magnitude.

Spin-unrestricted (polarized) calculations were also performed for the nitrogenated SWNTs. However, spin polarization was significant only for the case of N adatom chemisorption. The spin-polarized band structures, local DOS, and magnetism of singly N-chemisorbed SWNTs were presented in Sec. III D.

The structural stability and coalescence of two N adatoms chemisorbed on SWNTs into a N_2 molecule were presented in Sec. III E. The transition state energies of the coalescence processes were investigated using a generalized synchronous transition (GST) method.¹⁸ This method involved a linear synchronous transit (LST) maximization, followed by repeated conjugated gradient (CG) minimizations, and then quadratic synchronous transit (QST) maximizations and repeated CG minimizations until a transition state had been located (see Ref. 18 for details). The geometry optimization convergence threshold of the rms forces was set at $0.005 \text{ hartree/\AA}$. The “reactants” and “products” correspond

TABLE I. Deformation (δ), IP values, and magnetic moment (μ_B) of nitrogenated SWNTs.

Types of nitrogenation		δ	IP (eV/ \AA)	Magnetic moment (μ_B)
Zigzag (10,0) nanotubes	Pure	1.0	6.19	
	Substitution, C78N2	1.12	4.69	
	Pyridinelike doping, C72N6	1.13	4.85	
	Parallel chemisorption	1.07	4.77	0.72
	Perpendicular chemisorption	1.15	5.25	0.58
	$-NH_2$ functionalized	1.18	4.63	
Armchair (5,5) nanotubes	Pure	1.0	5.91	
	Substitution, C58N2	1.05	4.55	
	Pyridinelike doping, C52N6	1.28	4.79	
	Parallel chemisorption	1.08	4.60	0.61
	Perpendicular chemisorption	1.07	5.08	0.53
	$-NH_2$ functionalized	1.17	4.50	

to N-chemisorbed carbon structures and carbon structures with a N_2 molecule, respectively. The reactants and products are geometrically optimized before the full LST and/or QST search (see Tables IV and V for the relaxed reactants). The coalescence process was carried out for periodic systems of a graphene sheet and selected nanotubes.

III. RESULTS AND DISCUSSION

A. Atomic deformation, bond lengths, molecular orbital, and energetics

Figures 1 and 2 show the relaxed geometries of (10,0) and (5,5) nanotubes along with the distribution of the HOMO. Generally, it is noted that the cylindrically pristine nanotube is deformed to an ellipsoidal shape upon doping. A deformation factor (δ) is defined as the ratio of the major axis to the minor axis of the nanotubes. The δ values for the various types of nitrogenation are listed in Table I, together with the computed IP values.

It is noted that both (10,0) and (5,5) tubes have almost the same order of deformation factor δ for parallel chemisorption and $-NH_2$ functionalization. For pyridinelike doping, a (5,5) nanotube ($\delta \approx 1.28$) suffers a larger deformation than a (10,0) nanotube ($\delta \approx 1.13$), which could be due to the smaller diameter of (5,5) nanotube. On the other hand, direct substitution and perpendicular chemisorption cause more deformation in (10,0) nanotubes than in (5,5) nanotubes. Noteworthy, the sidewall of (5,5) nanotubes with chemisorbed N adatom is buckled, while (10,0) nanotubes are not so susceptible to buckling [compare Figs. 1(d) and 1(e) and Figs. 2(d) and 2(e)].

The bond lengths of the relaxed nanotubes at the vicinity of the nitrogen impurities are also displayed in Figs. 1 and 2. The C-N bond lengths of direct nitrogen substitution are determined to be $\sim 1.40\text{--}1.38 \text{ \AA}$ for the doped nanotubes both in Figs. 1 and 2. Due to the missing central C atom, the C-N

TABLE II. Formation energies of N-substituted and pyridinelike doped SWNTs.

Types of nitrogenation		E_f (eV) ^a
(10,0) nanotubes	Substitution, C79N1	1.78
	Substitution, C78N2	3.62
	Pyridinelike doping, C76N3	6.46
	Pyridinelike doping, C72N6	11.20
(5,5) nanotubes	Substitution, C59N1	1.71
	Substitution, C58N2	3.55
	Pyridinelike doping, C56N3	5.61
	Pyridinelike doping, C52N6	10.57

^aFormation energy of (10,0)NT, C76N3, is calculated as follows: $C80+3N \rightarrow C76N3+(1/80)C80$, i.e., $E_f=E[C76N3]+1/80E[C80]-E[C80]-3E[N]$. Similar energy calculations are performed for the other cases.

bond lengths of pyridinelike doping are determined to be $\sim 1.30\text{--}1.35$ Å, depending on the orientation, as compared to $1.42\text{--}1.47$ Å for the C-C bonds [see Figs. 1(c) and 2(c)]. For the chemisorbed N dopants, the C-N bond lengths of (5,5) tubes are about 1.45 Å (vs 1.51 Å, C-C bond) in the parallel positions and 1.37 Å (vs 2.10 Å, C-C separation in this case) in the perpendicular position. These bond length values are more locally distorted than (10,0) nanotubes [compare Figs. 2(d) and 2(e) and Figs. 1(d) and 1(e)]. Covalent -NH₂ functionalization results a C-N bond length of $\sim 1.47\text{--}1.48$ Å, while the surrounding C-C bonds are elongated to ~ 1.50 Å. Thus, it can be surmised that nitrogen impurities in CNTs produce their own local strains and results in the respective deformations. The relaxed structures of nitrogenated SWNTs relate well with experimental observations of compartmentalized and defective nitrogen-doped CNTs.^{4,19}

The effects of dissimilar nitrogenation on armchair and zigzag nanotubes are also reflected by the differences in the HOMO distribution. For instance, the HOMO of a nitrogen-substituted (10,0) nanotube is polarized at two opposite nitrogen dopants, while this is not the case for a nitrogen-substituted (5,5) nanotube [see Figs. 1(b) and 2(b)]. Pyridinelike doping causes the HOMO of doped (5,5) nanotube (NT) to be more concentrated at one side of the ellipsoidal ring [see Figs. 1(c) and 2(c)]. Another marked difference between doped (5,5) and (10,0) NTs is for the case of chemisorption of N adatoms at the perpendicular positions. The HOMO of a (10,0) nanotube is concentrated at the vicinity of the perpendicularly chemisorbed N adatom, while the HOMO of a (5,5) nanotube is roughly still distributed throughout the tube [compare Figs. 1(e) and 2(e)].

The formation energies (E_f) and absorption energies (E_a) of the nitrogenated SWNTs were given in Tables II and III, respectively. The energy cost to sp^2 substitute a C atom with a N atom in (10,0) and (5,5) nanotubes is 1.78 and 1.71 eV, respectively. On the other hand, it costs 6.46 and 5.61 eV to form pyridinelike doping in (10,0) and (5,5) nanotubes, respectively. The adsorption energies of exohedral N adatoms

TABLE III. Adsorption energies of chemisorbed N adatoms and -NH₂ on SWNTs.

Types of nitrogenation		E_a (eV) ^a
(10,0) nanotubes	Parallel chemisorption, C80N1	1.77
	Perpendicular chemisorption, C80N1	2.40
	-NH ₂ functionalization	2.34
(5,5) nanotubes	Parallel chemisorption, C60N1	1.49
	Perpendicular chemisorption, C60N1	2.75
	-NH ₂ functionalization	2.21

^aAdsorption energy is calculated as follows: $E_a=E(\text{CNT}+\text{impurity})-E(\text{CNT})-E(\text{impurity})$.

on SWNTs are dependent on the orientation of the C-N bridges relative to the tubular axes. The parallel chemisorption of SWNTs has lower absorption energy than the perpendicular chemisorption, which is understandable since the C-N bond lengths in the parallel positions are shorter than those in the perpendicular positions [1.45 vs 1.37 Å in (5,5) nanotube and 1.45 vs 1.39 Å in (10,0) nanotube]. The adsorption energy of -NH₂ on the outer surface of SWNTs is about 2.3 eV, which is comparable to the absorption energy of perpendicular N adatom chemisorption. The synthesis of N-doped carbon nanotubes is usually carried out at 700–900 °C using nitrogen-rich precursors for CVD processes.^{4,20,21} Spectroscopic studies and peak analysis revealed that C-N bonding of N-doped carbon nanotubes involved sp^2 , sp^3 -typed, and intercalated N₂ as well, which might be attributed to sp^2 substitution of C atom with a N atom, pyridinelike doping, and molecular N₂, respectively. The relatively high synthesis temperature and use of catalysts might provide sufficient energies to form pyridinelike defects in N-doped carbon nanotubes, though the formation energies of pyridinelike defects are higher than those for sp^2 substitution. Furthermore, the decomposition of nitrogen-rich precursors might generate N adatoms which chemisorbed on the graphitic layers of carbon nanotubes and subsequently coalesce to form intercalated N₂ molecules (see Sec. III E). Pristine carbon nanotubes can also be modified with nitrogen impurities using N ion irradiation N₂/NH₃ plasma treatment. Khare *et al.*^{7,8} showed that the -NH₂ functional group is mostly attached to carbon nanotube after N₂/NH₃ plasma treatment, whereby the absorption energy of ~ 2 eV is supplied by the plasma. Atomistic simulation study¹⁰ of N ion implantation into carbon nanotubes showed that up to 40% of the N ion irradiation results in sp^2 substitution of the nanotube C network, and annealing the N-bombarded nanotubes further increases the sp^2 N dopants. Thus, the synthetic conditions, nitrogen plasma treatment, and N ion implantation can be utilized to favorably control the types of N impurities in carbon nanotubes. This, in turn, implied that the electronic properties of carbon nanotubes can be experimentally tuned according to the types of N impurities introduced, and this is important for nanotube-based electronic devices. The electronic properties of different nitrogenated SWNTs are presented in Sec. III B.

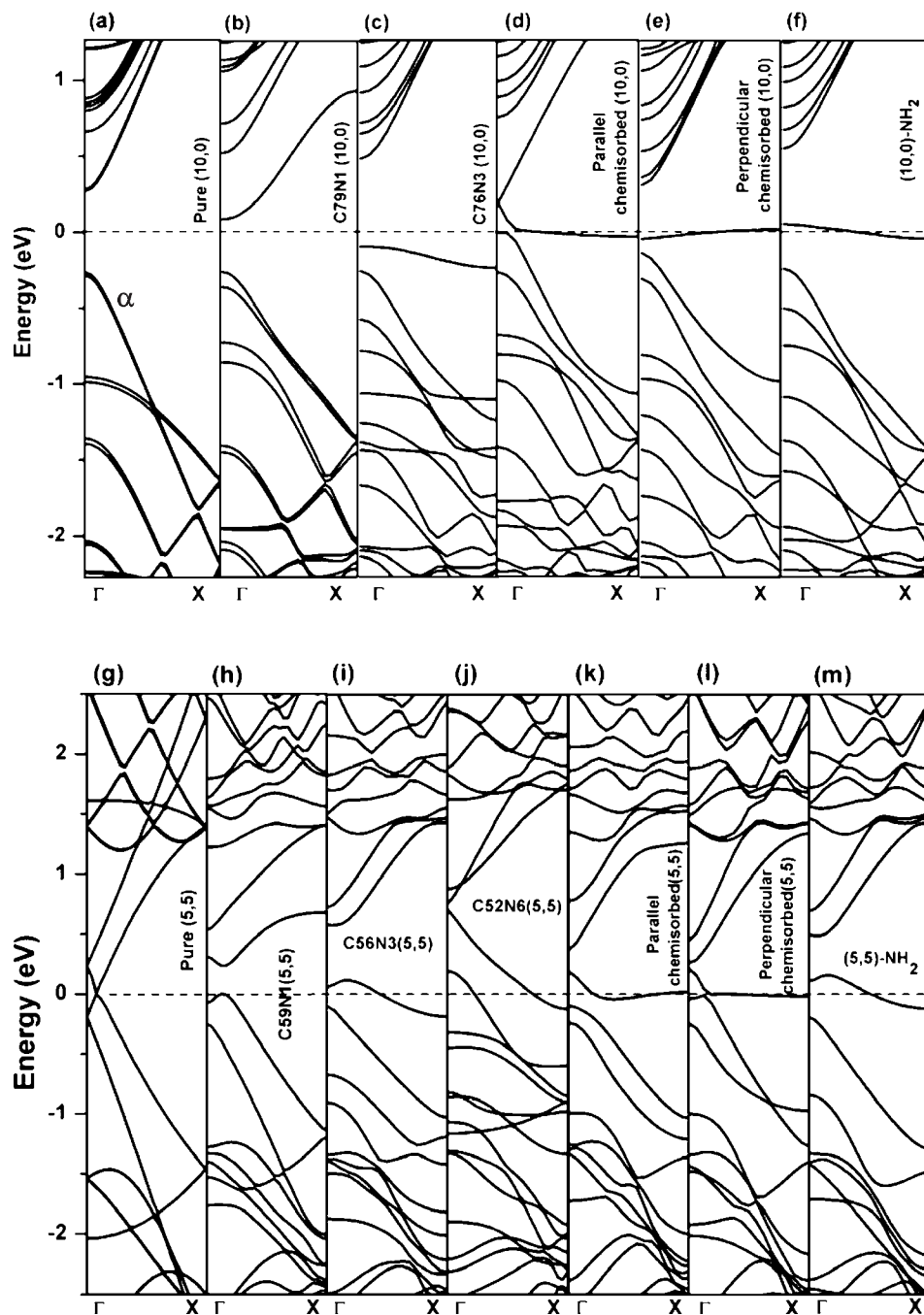


FIG. 3. Band structures of (10,0) and (5,5) nanotubes: [(a) and (g)] pure, [(b) and (h)] N substitution, [(c), (i), and (j)] pyridinelike doping, [(d) and (k)] chemisorption at parallel position, [(e) and (l)] chemisorption at perpendicular position, and [(f) and (m)] -NH_2 functionalization. (a)–(f) and (g)–(m) are for (10,0) and (5,5) nanotubes, respectively. The Fermi level is represented by the dotted horizontal lines.

B. Spin-restricted electronic properties

Figures 3(a)–3(f) compare the electronic band structures of pure and nitrogenated (10,0) nanotubes in the vicinity of the Fermi level. A pure zigzag (10,0) SWNT has a D_{10h} symmetry, and most of the energy levels are doubly degenerate due to the rotational point group C_n . Figure 3(a) shows the band structure of a pure (10,0) nanotube, which is very similar to that in Ref. 22. The topmost valence band and bottom conduction band correspond to the big π -bonding and π^* -antibonding states along the ring of the tube, respectively. Upon nitrogenation, the degeneracies of the energy bands of (10,0) nanotubes are removed. That is, the presence of nitrogen impurities causes the α band to split. The split-

ting of the band is most prominent for parallel chemisorption [Fig. 3(d)]. A new band develops just below the Fermi level for pyridinelike doping [p type, Fig. 3(c)], while a new band develops in the middle of the Fermi level for -NH_2 functionalization [Fig. 3(f), still regarded as p -type doping due to the presence a small gap between the new energy band and the valence band]. Direct nitrogen substitution creates a new band just above the Fermi level (i.e., below the lowest conduction bands), which exemplifies an n -type doping. Band structure study reveals a significant difference between parallel and perpendicular chemisorptions. A new energy band cuts across the Fermi level for parallel chemisorption and makes the doped (10,0) nanotube metallic. On the other hand, a new energy band is developed at the Fermi level and

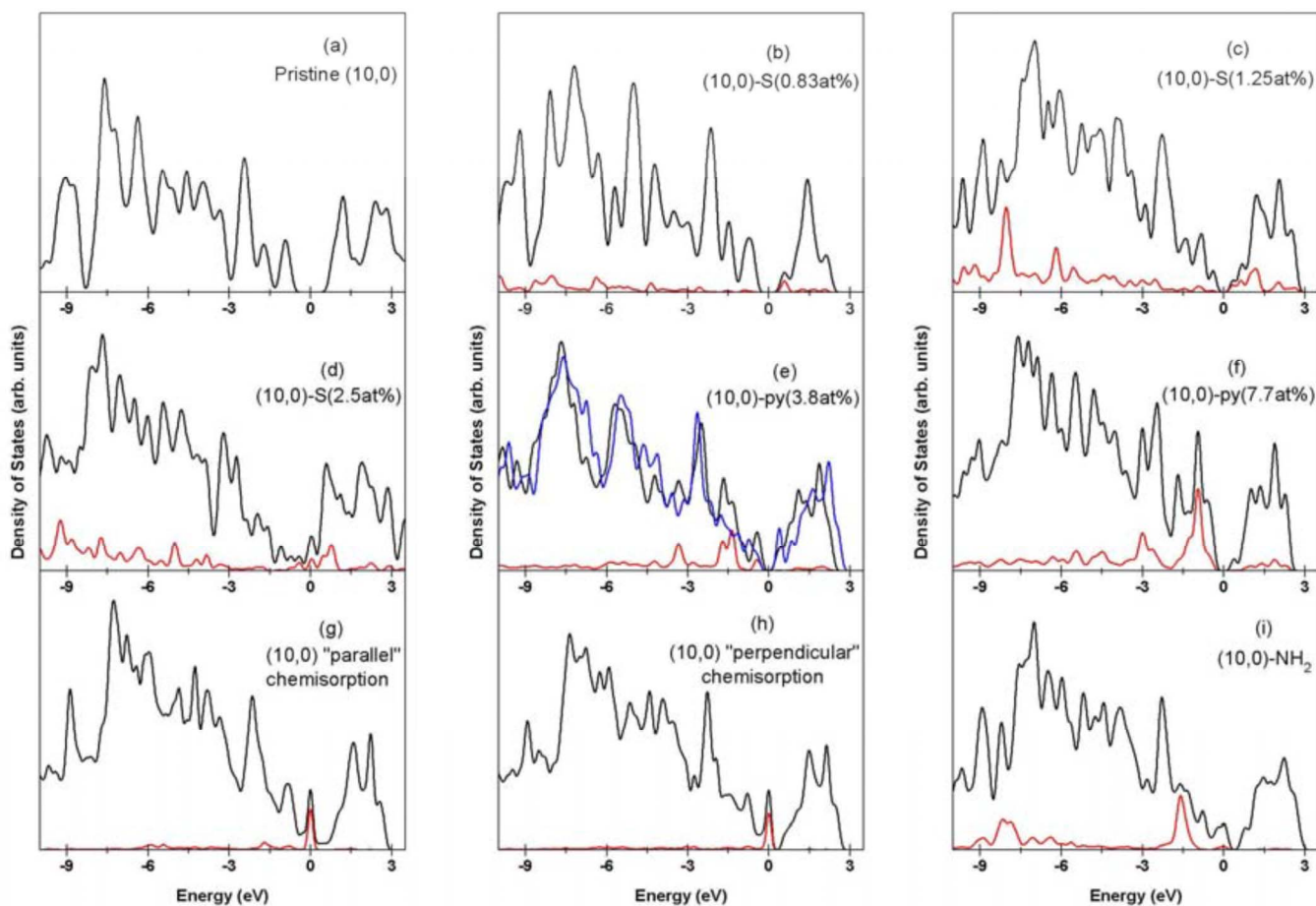


FIG. 4. (Color online) Total density of states (TDOS) of (a) pristine (10,0) nanotube, [(b)–(d)] nitrogen substitution, [(e) and (f)] pyridineline doping, [(g) and (h)] chemisorption of N adatoms, and (i) $-\text{NH}_2$ functionalization. Projected DOS of nitrogen impurities and TDOS of undoped (10,0) nanotube with monovacancy are indicated as red (light gray) line and blue (dark gray) line, respectively. The Fermi level is at 0 eV. A 120 atoms/cell supercell is used to compute case (b) substitution.

there is narrowing of the gap between the new band and the conduction band for the perpendicular chemisorption (considered as n type).

Our band structure study is consistent with Zhao *et al.*²³ who have investigated the band structures of SWNTs with covalent sidewall functionalization (e.g., COOH, OH, F, H, CH_3) and pointed out the marked difference between covalent functionalization and substitutional doping. As in the case of semiconducting (10,0) nanotubes, substitutional doping does not disturb the sp^2 hybridization of the π electrons and the N impurity states contribute mainly to the minimum of the conduction band, while tube-impurity covalent interaction creates an impurity state on the top of the valence band due to sp^3 defect. As indicated in Figs. 1(b) and 1(f), the C-C bond lengths of $-\text{NH}_2$ functionalized nanotubes are elongated to ~ 1.50 Å (sp^3 defect), while the C-C bond lengths of nitrogen substitution are ~ 1.40 Å (sp^2).

The electronic band structures of pure and doped (5,5) nanotubes are displayed in Figs. 3(g)–3(m). The π - π^* band crossing of the pure (5,5) metallic tube is disturbed by the presence of N impurities. Small band gaps open up between the conduction and valence bands, which are attributed to the breaking of the armchair nanotube mirror symmetry due to

the tube-impurity interaction. The opening of small gaps has also been reported for covalently functionalized and Cu-adsorbed metallic nanotubes.^{23,24} In addition, (5,5) nanotube with two pyridine doping [i.e., C52N6 as displayed in Fig. 2(c)], which has even number of electrons, remains metallic. As shown in Fig. 3(j), these (5,5) nanotubes (C52N6) have two bands that can be seen crossing the Fermi level.

In Fig. 4, we present the electronic DOS of pristine and nitrogenated (10,0) nanotubes. At low concentration of dopants (0.83 at. %), direct substitution of nitrogen narrows the band gap and slightly shifts the Fermi level toward the conduction band. Projected DOS of the nitrogen impurity state indicated that an impurity state is developed at ~ 0.5 eV in the conduction bands [n -type doping, see Fig. 4(b)], but complicated hybridization also occurs at the higher energy regions of the valence bands, along with the removal of the double degeneracies as indicated in the band structures. At higher level of doping [see Figs. 4(c) and 4(d)], the band gap continues to narrow and eventually filled with impurity states at higher concentration of dopants. For instance, N-substituted (10,0) nanotubes of 2.5 at. % become metallic due to the finite states at the Fermi level [see Fig. 4(d)].

Although pyridineline doping has a relatively higher concentration of dopants (compare ~ 3.8 at. % [Fig. 4(e)] of py-

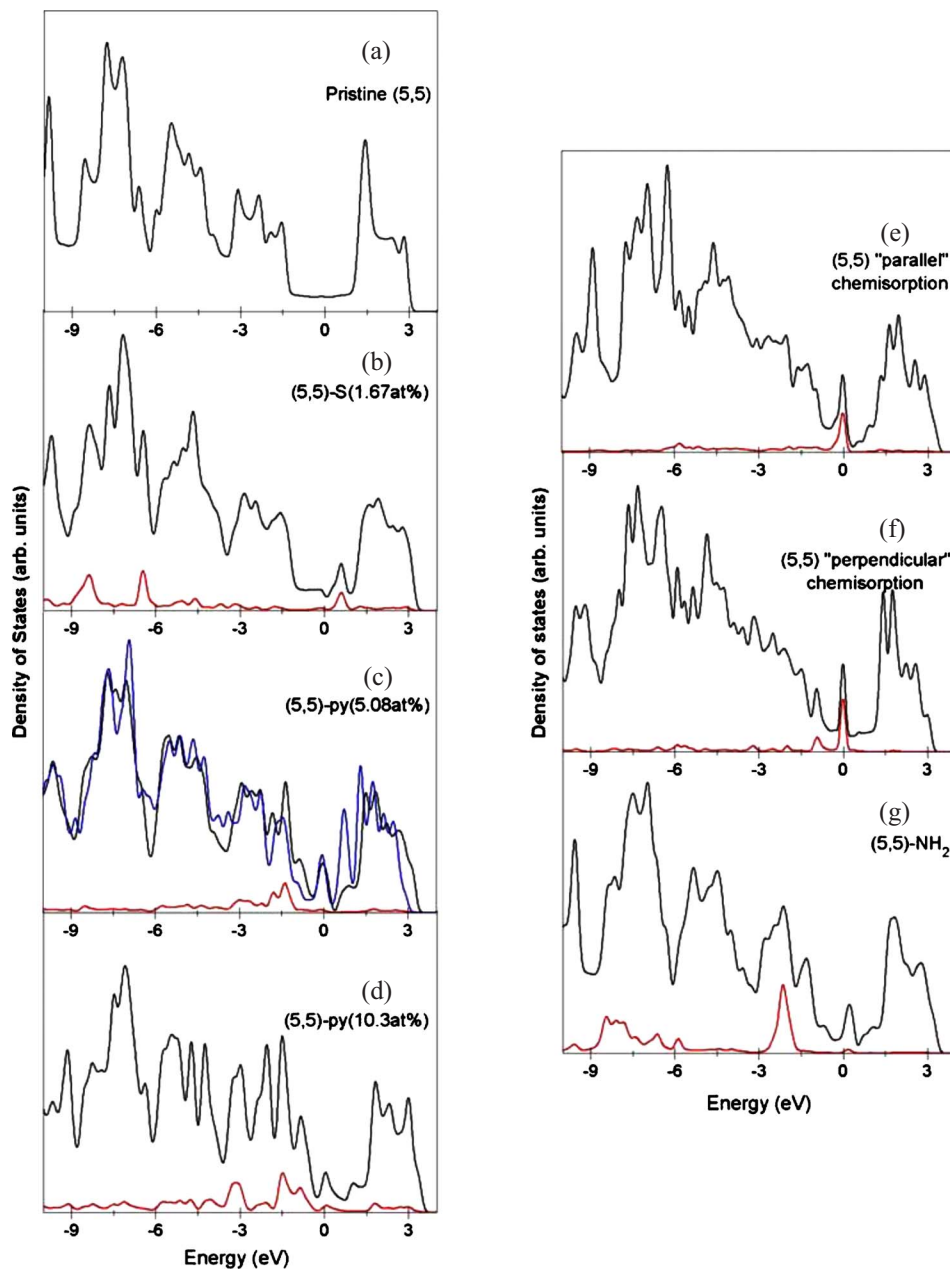


FIG. 5. (Color online) TDOS of (a) pristine (5,5) nanotube, (b) nitrogen substitution, [(c) and (d)] pyridinelike doping, [(e) and (f)] chemisorption of N adatoms, and (g) -NH_2 functionalization. Projected DOS of nitrogen impurities and TDOS of undoped (5,5) nanotube with monovacancy are indicated as red (light gray) line and blue (dark gray) line, respectively. The Fermi level is at 0 eV.

ridinelike doping vs 2.5 at. % [Fig. 4(d)] of N substitution), the band gap remains though narrower. At even higher concentration of pyridinelike doping [7.7 at. %, Fig. 4(f)], the doped (10,0) nanotube still remains as a narrow gap semiconductor. This is in contrast to direct substitution (~ 2.5 at. %) which can yield metallic nanotubes at higher impurity concentrations. However, our calculated DOS of (10,0) nanotube with pyridinelike doping does not agree to the calculation of Czerw *et al.*,¹⁷ which was based on tight-binding method, and concluded that nanotubes with pyridinelike nitrogen doping behave as donor-type doping. Kang and Jeong²⁵ also calculated SWNTs with pyridinelike nitrogen doping and concluded that the resultant SWNTs possessed acceptorlike impurities due to the presence of lone pair states. Our calculated DOS of (10,0) tubes with pyridinelike nitrogen doping [Fig. 4(e)] agrees well to the results of Kang and Jeong.²⁵ To understand the role of nitrogen impurities in

the pyridinelike vacancy, we have also computed the DOS of a (10,0) tube with monovacancy but without nitrogen dopants [see Fig. 4(e), blue (dark gray) line]. The relaxed geometry of such a (10,0) tube with vacancy shows a similar deformation and, interestingly, a reduction of band gap which matches quite closely to (10,0) tube with pyridinelike nitrogen doping. Therefore, the effects of the nitrogen dopants in pyridinelike doping do not significantly modify the band gap, but noticeable increase (decrease) in the density of states at about -0.4 , -1.5 , and -3.3 eV (-4.4 and -6.7 eV) in the valence band. In other words, the pyridinelike doping causes the zigzag nanotube to become a narrow gap semiconductor, and the projected DOS of the N dopants shows that the impurity states are located ~ 0.4 eV below the Fermi level (Kang and Jeong²⁵ obtained impurity states at ~ 0.5 eV below the Fermi level) and thus can be regarded as acceptorlike impurities.

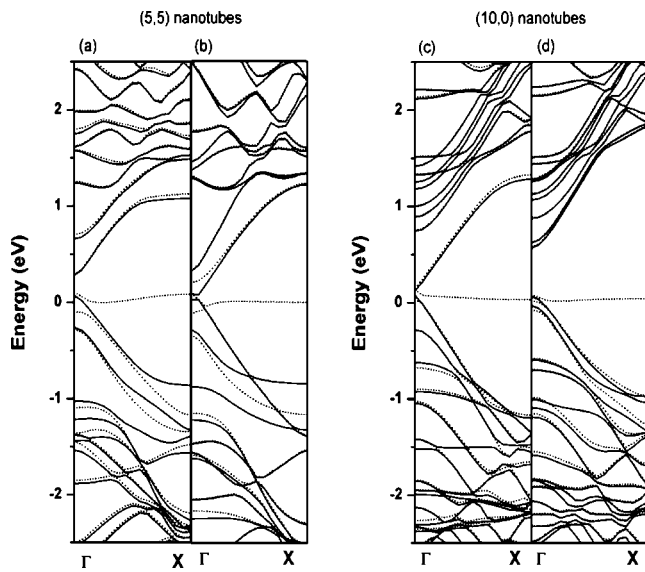


FIG. 6. Spin-polarized band structures of singly N-chemisorbed SWNTs in [(a) and (c)] parallel and [(b) and (d)] perpendicular positions. Majority spin and minority spin electrons are denoted by solid and dotted lines, respectively.

The exohedral chemisorption of a single N adatom onto a (10,0) nanotube significantly alters the band gap. As shown in Fig. 4(h), the projected DOS of the exohedrally perpendicular chemisorbed N adatom indicates that it is behaving as *n*-type dopant, which is in contrast to endohedrally chemisorbed N adatom (*p* type).²⁶ However, a closer inspection of chemisorption in the parallel position indicates that the (10,0) nanotubes show metallic behavior, which is consistent with the band structure study [Fig 3(d)].

We also noted that the DOS profile of $-NH_2$ functionalization of a (10,0) nanotube is reminiscent of $-OH$ functionalization.²² The projected DOS of the $-NH_2$ moiety shows that a weak impurity state is located at the Fermi level, and a stronger impurity state is located at ~ 1.2 eV below the Fermi level [Fig 4(i)]. It is considered that a $-NH_2$ moiety behaves as an acceptor impurity. Zhao *et al.*²³ showed that regardless of the types of covalent sidewall functionalization of SWNTs, sp^3 hybridization between the functional group and nanotube induces an impurity state near the Fermi level.

The electronic densities of states of pure and nitrogenated armchair (5,5) nanotubes are displayed in Fig. 5. The DOS of pure (5,5) tube exhibits a finite DOS at the Fermi level, which renders it metallic. Figure 5(b) shows that nitrogen substitution develops an impurity state below the conduction

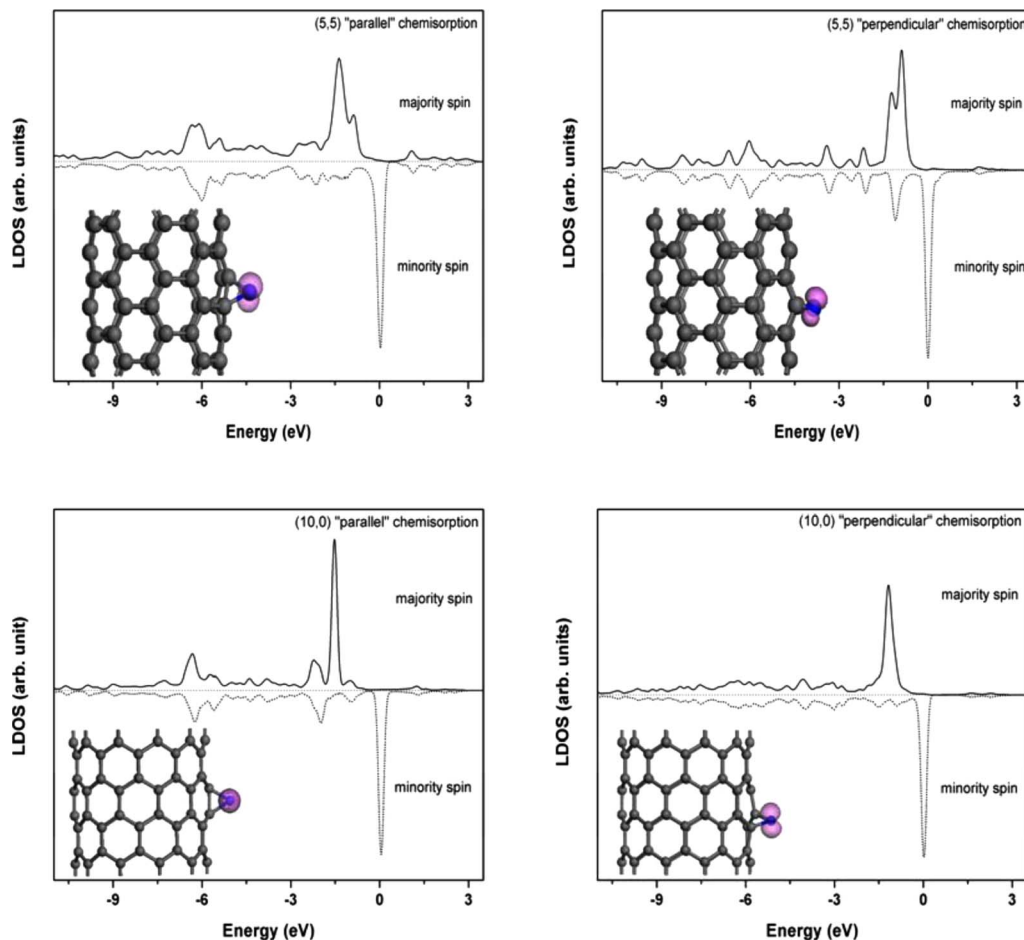


FIG. 7. (Color online) Spin-polarized local density of states of a single N adatom chemisorbed on (10,0) and (5,5) nanotubes. The pink isosurface of the spin density is set at the value of $0.05e/\text{\AA}^3$. The gray and blue spheres represent C and N atoms, respectively.

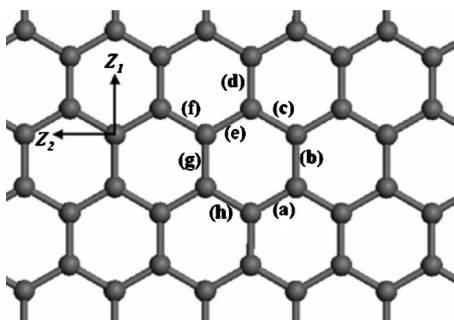


FIG. 8. Possible configurations of two neighboring N adatoms chemisorbed on a graphene sheet. Z_1 and Z_2 directions represent the tubular axes of zigzag (10,0) and armchair (5,5) nanotubes, respectively.

bands (~ 0.6 eV above the Fermi level), and a small valley is noted near the Fermi level. The presence of small valleys in the vicinity of the Fermi level is also observed for other nitrogenated (5,5) tubes, and this is mainly due to the broken mirror symmetry of the π - π^* band crossing as discussed in the band structure studies. For the case of the (5,5) tube with pyridinelike doping [Figs. 5(c) and 5(d)], a peak at the Fermi level is observed. However, the projected DOS of the nitrogen impurities shows that the impurity states are mainly located below the Fermi level ~ 1.3 eV, and the impurity states at Fermi level are very weak for ~ 5 at. % doping level. Likewise, we have also computed the DOS of (5,5) tubes with monovacancy (without N impurities), and their DOS also shows a sharp peak at the Fermi level [see Fig. 5(c), blue (dark gray) line]. Thus, the observed DOS peak at the Fermi level of the pyridinelike nitrogenated (5,5) tube is due to the vacancy and not to the nitrogen dopants. The DOS of pyridinelike nitrogenated (5,5) tube is quite similar to the (5,5) tube with pyridine vacancy (without N impurities), except for a marked decrease (slight increase) at about -3.5 and 0.7 eV (-0.8 and -1.3 eV). The DOS of chemisorption of nitrogen adatoms and $-NH_2$ functionalization of (5,5) nanotubes is quite similar to the case of doped (10,0) nanotubes.

C. Ionization potential energies

Although most theoretical calculations of field emission (FE) properties of carbon nanotubes are performed with finite clusters, the aim of using supercell geometries in this paper is to compare qualitatively the FE properties among the nitrogenated nanotubes. The IP values of the nitrogenated SWNTs are displayed in Table I. The IP value of a pure (10,0) nanotube is calculated to be 6.19 eV/Å, which is slightly lower than the IP value of 6.4 eV/Å for a closed capped (5,5) nanotube reported by Maita *et al.*²⁷ The IP values of nitrogenated (10,0) nanotubes in increasing order are 4.63 eV ($-NH_2$ functionalization), 4.69 eV (substitution), 4.77 eV (parallel chemisorption), 4.85 eV (pyridinelike doping), and 5.25 eV (perpendicular chemisorption). A similar trend of IP values is also noted for nitrogenated (5,5) nanotubes, but the IP values are lower than those for the nitrogenated (10,0) NTs. Therefore, $-NH_2$ functionalization and nitrogen substitution might be advantageous to the field

emission properties of carbon nanotubes. Our results indicate that the field emission properties of pristine carbon nanotubes can be experimentally improved using N_2/NH_3 plasma treatment and N ion implantation to modify carbon nanotubes with NH_2 moiety and sp^2 substitution, respectively.

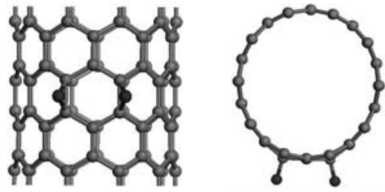
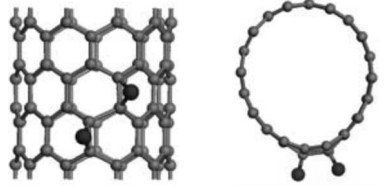
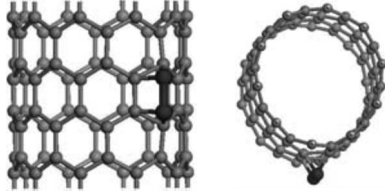
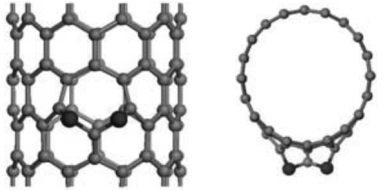
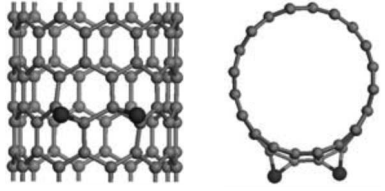
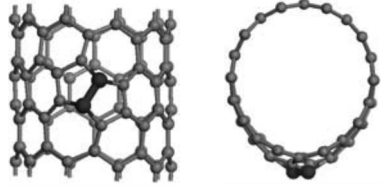
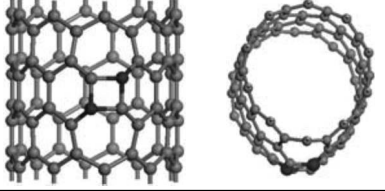
D. Spin-unrestricted electronic properties of singly N-chemisorbed single-walled carbon nanotube

We have also evaluated the electronic properties of the nitrogenated SWNTs using spin-unrestricted calculations. The spin-unrestricted (polarized) band structures and DOS of the nitrogenated SWNTs are very similar to the spin-restricted calculations, except for nitrogen chemisorptions. Hence, the spin-polarized band structures and local DOS of the singly N-chemisorbed SWNTs are displayed in Figs. 6 and 7, respectively. It is noted that the minority spin band structures are quite similar to the spin-restricted band structures, while the majority spin band structures are different. On the basis of Fig. 7, majority spin local density of states (LDOS) peaks are located at about 0.9 – 1.5 eV below the Fermi level, while minority spin LDOS peaks are located at the Fermi level. Furthermore, the distribution of the spin polarization (insets of Fig. 7), which comes from the p orbital of the N adatoms, is perpendicular to the C-N-C plane. This resembles the case of a N adatom chemisorbed on a graphene sheet, whereby the spin distribution is also perpendicular to the C-N-C plane.¹² The magnetic moments (μ_B) of the chemisorbed (10,0) and (5,5) nanotubes are also tabulated in Table I. The magnitude of the magnetic moment depends on the positions of the chemisorbed N adatoms and the chiralities and diameters of the SWNTs. A parallel chemisorption has a larger magnetic moment than a perpendicular chemisorption. Also, the magnitudes of the magnetic moment of a semiconducting (10,0) nanotube are larger than those of a metallic (5,5) nanotube. Ma *et al.*¹² reported that the magnitude of the magnetic moment of nitrogenated graphite is related to the coupling of the N adatom's p orbital with the carbon π orbital. That is, a larger coupling of the p - π orbital yields a smaller magnetic moment. The broken C-C bond in the perpendicular chemisorption may have given rise to a stronger coupling between the N adatom's p orbital and the carbon π orbital, and therefore perpendicular chemisorption has a smaller μ_B than parallel chemisorption. Likewise, the more delocalized π orbital of a metallic (5,5) nanotube couples more strongly to the N adatom's p orbital than a semiconducting (10,0) nanotube. Therefore, N-chemisorbed (5,5) nanotube has a smaller magnitude of magnetic moment than (10,0) nanotube.

E. Structural stability and coalescence of two neighboring chemisorbed N adatoms

In the case of high density nitrogen chemisorption, the stability of the defects with respect to recombination into N_2 molecules is an important issue to study. For example, intercalation of N_2 molecules between the graphitic layers of nanotubes has been experimentally observed.^{20,21} Thus, in this section, we examine the structural stability of two

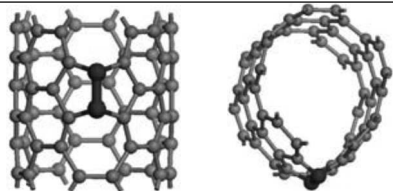

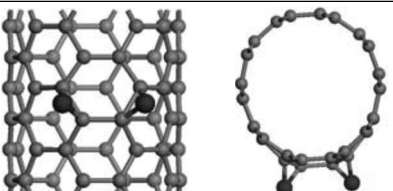
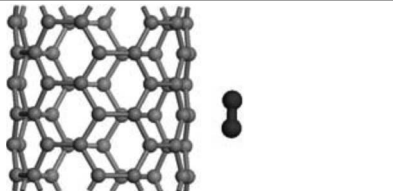
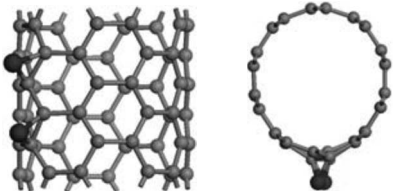
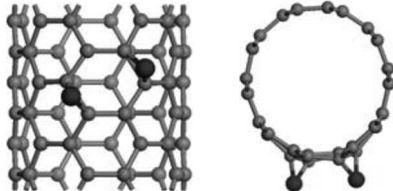
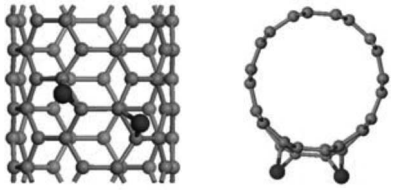
TABLE IV. Relaxed zigzag (10,0) SWNTs with two chemisorbed N adatoms. $(X\cdots X)$ and $(Y-Y)$ denote atom-to-atom separation length and bond length, respectively. E_T is the total energy of the system in units of Hartree. $\angle\text{CNC}$ denotes the average bond angle. Positions of N adatoms and carbon-carbon lengths are labeled according to Fig. 8.

	Relaxed configurations	Remarks
"Parallel" chemisorption		<u>(g)-(b) position</u> (N \cdots N) = 3.182Å (C-C) = 1.513Å (C-N) = 1.460Å $\angle\text{CNC} = 62.381^\circ$ $E_T = -3155.478503\text{Ha}$
		<u>(g)-(d) position</u> (N \cdots N) = 3.200Å (C-C) = 1.481Å (C-N) = 1.480 / 1.392Å $\angle\text{CNC} = 61.996^\circ$ $E_T = -3155.4925991\text{Ha}$
"Perpendicular" Chemisorption		<u>(c)-(a) position</u> (N-N) = 1.566Å (C-C) = 1.575Å (C-N) = 1.492 / 1.546Å $\angle\text{CNC} = 62.425^\circ$ $E_T = -3155.5578901\text{Ha}$
		<u>(c)-(e) position</u> (N \cdots N) = 2.252Å (C \cdots C) = 2.164Å (C-N) = 1.374 / 1.395Å $\angle\text{CNC} = 102.884^\circ$ $E_T = -3155.5446995\text{Ha}$
		<u>(c)-(f) position</u> (N \cdots N) = 3.554Å (C-C) = 1.611Å (C-N) = 1.414 / 1.459Å $\angle\text{CNC} = 68.171^\circ$ $E_T = -3155.4927862\text{Ha}$
		<u>(c)-(h) position</u> (N-N) = 1.491Å (C \cdots C) = 2.408Å (C-N) = 1.383 / 1.429Å $\angle\text{CNC} = 117.708^\circ$ $E_T = -3155.6035269\text{Ha}$
		<u>(f)-(h) position</u> (N \cdots N) = 1.998Å (C \cdots C) = n.a. (C-N) = 1.390/ 1.408Å $\angle\text{CNC} = \text{n.a.}$ $E_T = -3155.6149498\text{Ha}$

neighboring N adatoms chemisorbed on SWNT surfaces and the coalescence process into a N_2 molecule. We assume that the two N adatoms on a graphitic surface must be sufficiently close to each other before they coalesce to form a N_2 molecule. In Fig. 8, various positions for holding two neighboring N adatoms on a graphene sheet are considered and la-

beled from (a) to (h). Z_1 and Z_2 vectors in the figure represent the tubular axes of (10,0) and (5,5) nanotubes, respectively. The structures with two neighboring N adatoms at the assumed positions are allowed to relax fully. The relaxed structures of SWNTs with two N adatoms are schematically presented in Tables IV and V, together with the calculated

TABLE V. Relaxed armchair (5,5) SWNTs with two chemisorbed N adatoms. ($X\cdots X$) and ($Y-Y$) denote atom-to-atom separation length and bond length, respectively. E_T is the total energy of the system in units of Hartree. $\angle\text{CNC}$ denotes the average bond angle. Positions of N adatoms and carbon-carbon lengths are labeled according to Fig. 8.

	Relaxed configurations	Remarks
"Perpendicular" chemisorption		<u>(g)-(b) position</u> (N-N) = 1.537Å (C...C) = 2.309Å (C-N) = 1.440Å $\angle\text{CNC} = 106.630^\circ$ $E_T = -2394.0002572\text{Ha}$
		<u>(g)-(d) position</u> (N...N) = 3.524Å (C...C) = 2.137Å (C-N) = 1.391 / 1.350Å $\angle\text{CNC} = 102.377^\circ$ $E_T = -2393.8851250\text{Ha}$
"Parallel" Chemisorption		<u>(c)-(a) position</u> (N...N) = 3.251Å (C-C) = 1.518 / 1.519Å (C-N) = 1.441 / 1.468Å $\angle\text{CNC} = 62.977^\circ$ $E_T = -2392.8118746\text{Ha}$
		<u>(c)-(e) position</u> (N-N) = 1.109 (free N ₂) (C...C) = n.a. (C-N) = n.a. $\angle\text{CNC} = \text{n.a.}$ $E_T = -2394.0731784\text{Ha}$
		<u>(c)-(f) position</u> (N...N) = 2.903Å (C-C) = 1.515Å (C-N) = 1.436 / 1.471Å $\angle\text{CNC} = 62.809^\circ$ $E_T = -2393.8028447\text{Ha}$
		<u>(c)-(h) position</u> (N...N) = 3.128Å (C-C) = 1.566Å (C-N) = 1.437 / 1.458Å $\angle\text{CNC} = 65.525^\circ$ $E_T = -2393.7949533\text{Ha}$
		<u>(f)-(h) position</u> (N...N) = 3.444Å (C-C) = 1.506Å (C-N) = 1.435 / 1.479Å $\angle\text{CNC} = 62.256^\circ$ $E_T = -2393.8252540\text{Ha}$

bond lengths (or atom-to-atom separation distance), bond angles, and total energies.

Most of the relaxed structures in Tables IV and V are very similar to their counterparts of single N adatom chemisorption, except that the number of N adatoms increases from 1 to 2. That is, the bridged C-C bonds are also broken for

perpendicular chemisorption [see (c)-(e) position of (10,0) tube and (g)-(d) position of (5,5) tube], with the exception of perpendicular (c)-(f) position of (10,0) nanotube, whereby the bridged C-C bonds are prevented from being broken due to the "squeezing" of the C-C at position (e). The relaxation of the "parallel" chemisorptions of two N adatoms can also

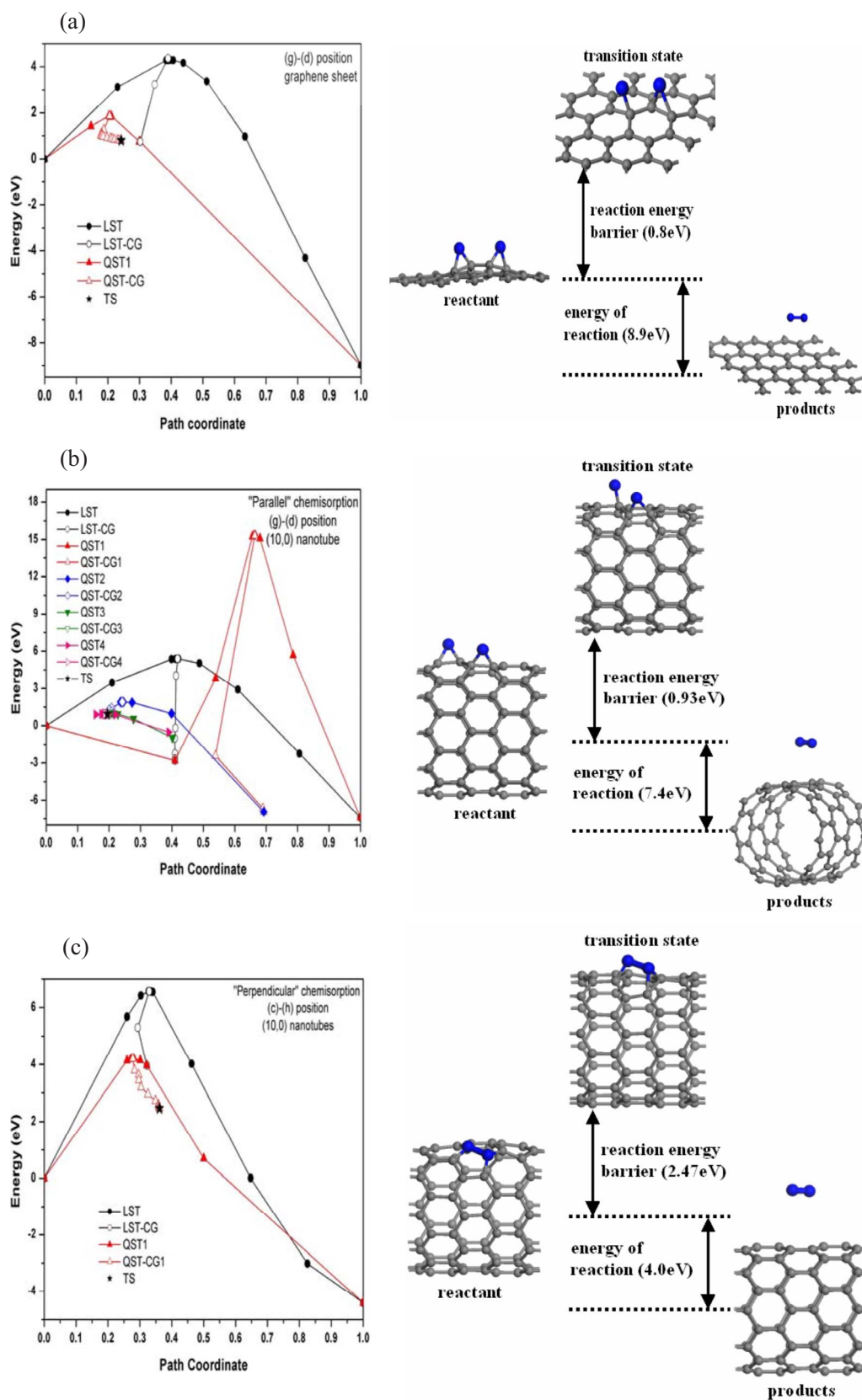


FIG. 9. (Color online) Energy versus path coordinate during transition state search. The path coordinate "0" represents the reactant (SWNT with two chemisorbed N atoms), while path coordinate "1" represents the products (SWNT+a free N₂ molecule). Cases (a), (b), and (c), and (d), (e) are the transition state search and energy diagrams for a graphene sheet, (10,0) nanotube, and (5,5) nanotube, respectively. Energy diagrams are not drawn to scale.

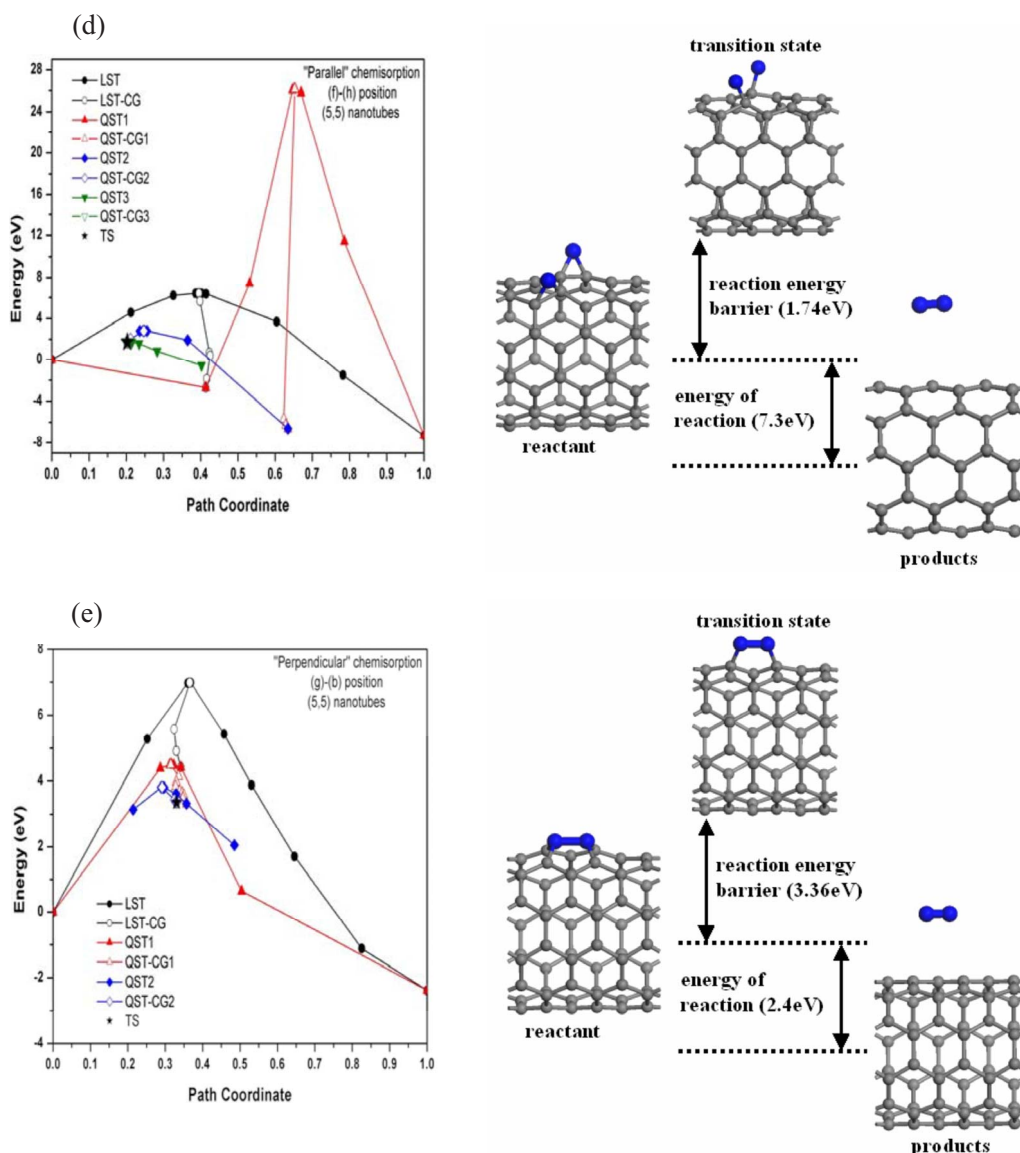


FIG. 9. (Continued).

be anticipated from the results of single chemisorption [see (g)-(b) and (g)-(d) positions of (10,0) tubes and (c)-(a), (c)-(f), (c)-(h), and (f)-(h) positions of (5,5) tubes].

However, some of the structures in Tables IV and V are unexpected and dissimilar to the above listed ones. Their structures are more complex and richer in defects, as expatiated below. In the first case of this series, the (5,5) (c)-(e) (parallel chemisorption) in Table V, the relaxed structures yield a pristine (5,5) nanotube and a N₂ molecule. In comparison with other parallel positions of (5,5) nanotube, the N adatoms in the (c)-(e) position can be considered as unstable and, upon relaxation, can form N₂ molecule. For the two N adatoms chemisorbed at the (c)-(e) positions in a (10,0) nanotube (perpendicular chemisorption), however, the relaxed structures yield a (10,0) nanotube chemisorbed with two N adatoms and two broken C-C bonds. Geometry optimization revealed that the nitrogen-nitrogen repulsion had caused the two chemisorbed N adatoms of (5,5) nanotube at (c)-(e) position to elongate their C-N bonds and transform

the C-N bridges to become C-N single bonds. The two C-N single bonds are able to rotate and form an intermediate N-N bond before breaking the C-N bonds and escaping as a free N₂ molecule. However, for chemisorbed two N adatoms on (10,0) at (c)-(e) positions (perpendicular), the broken C-C bond kept the N-to-N atoms farther apart, not forming a free N₂. In the second cases of the series, the formation of N-N bond is possible at some of the perpendicular positions [see (c)-(a) and (c)-(h) positions for (10,0) tube and (g)-(b) position for (5,5) tube], which is due to the breaking or elongating of bridged C-C bonds and allowing the two N adatoms to come closer together to form a N-N bond. Consequently, pentagon-heptagon pair defects are formed on these SWNTs if the bridged C-C bonds are broken. These N-N bond lengths are ~1.49–1.56 Å, which is longer than the bond length of a free N₂ molecule (1.11 Å), but close to the N-N bond lengths of boron nitride nanotubes with pentagon-heptagon defects.²⁸ In the third case of the series, the perpendicular (f)-(h) positions of (10,0) tube consist of fourfold and

sevenfold ring defects, and the total energy is the lowest among the positions considered (see Table IV). Besides breaking the C-C bonds at positions (f) and (h) (see Fig. 8), the C-C bond at position (g) is torn apart due to the formation of a weak N-N bond which is subsequently broken as well. The relaxed C-N bond is ~ 1.40 Å, which is close to the C-N bond length observed in sp^2 substitution. Bettinger *et al.*²⁹ have investigated a 4774 defect (fourfold and sevenfold ring defects) in carbon nanotube, but a 5775 defect (fivefold and sevenfold ring defects, or simply Stone-Wales defect) is more stable. Although the relaxed perpendicular position (f)-(h) of (10,0) nanotube does not resemble the 4774 defect, our results suggest that the presence of N impurities can give rise to a single fourfold and two sevenfold ring defects in semiconducting carbon nanotubes. Furthermore, the relaxed structures of the N dopants are no longer protruding out the SWNT surface and substantially different from other cases of chemisorption.

On the basis of geometry optimization of the SWNTs with two neighboring N adatoms, we have demonstrated the important effects of the relative adsorption positions of N adatoms and the nanotube chiralities on the tube structural stability and the resultant defects.

We have applied the GST method,¹⁸ as implemented in DMOL³ code, to search the transition state of the coalescence process of two chemisorbed N adatoms. We tested the method for the case of a graphene sheet with two chemisorbed N adatoms. As shown in Fig. 9(a), the transition state consists of one N adatom bridging over the C-C bond while the other forming a single bond with the graphene sheet. Furthermore, the two chemisorbed N adatoms had severely distorted the graphene sheet. The N···N separation of this transition state is 2.0 Å and the reaction energy barrier is 0.80 eV, which is in good agreement with a previous report.¹² Therefore, we had conducted the LST and/or QST search for selected nitrogenated SWNTs using the same procedure. For (10,0) nanotubes, chemisorptions at positions (g)-(d) and (c)-(h) were chosen because these positions had the lowest total energies. However, (c)-(h) position of (10,0) is preferred over (f)-(h) position because it still retained the C-N bridgelike bonds. Similarly, (f)-(h) and (g)-(b) positions were chosen for nitrogenated (5,5) nanotubes since these positions had the lowest total energies. The coalescence processes of two N adatoms chemisorbed on SWNTs into a free N₂ molecule are presented in Figs. 9(b), 9(c), 9(d), and 9(e). It is noted that the reaction energy barrier of SWNTs is

higher than that of the graphene sheet. The coalescence of N adatoms with perpendicular chemisorption is less complex than the parallel chemisorption (involving fewer numbers of LST and/or QST search). The reaction energy barrier (energy of reaction) of the perpendicular chemisorption is much higher (lower) than that of the parallel chemisorption. This implied that it is more difficult to coalesce two chemisorbed N adatoms into the N₂ molecule in the perpendicular positions than in the parallel positions. The reaction energy barrier of (10,0) nanotube is ~ 0.8 eV lower than that of (5,5) nanotube, which might be due to the larger curvature of (10,0) nanotube and stronger C-N bonding of (5,5) nanotube. It can be surmised that the intercalation of N₂ molecules in nanotube interlayer is most likely due to the coalescence of N adatoms chemisorbed in parallel configurations.

IV. CONCLUSIONS

The structural and electronic properties of nitrogenated (5,5) and (10,0) are studied using first-principles methods. The effects of different types of nitrogenation have been elucidated from the band structures, density of states (DOS), and molecular orbital. Our calculations indicate that the substitutional nitrogenation, -NH₂ functionalization, as well as chemisorption will convert semiconducting (10,0) nanotubes (~ 0.7 eV band gap) into metallic, while pyridineline nitrogenation can only shorten the band gap, converting the (10,0) tube to narrow gap (< 0.2 eV) semiconductors. For metallic (5,5) nanotubes, the N doping is shown to significantly enhance the state density at the vicinity of Fermi level, which can enhance its chemical activity. Comparing among the calculated ionization potentials of the various nitrogenated nanotubes indicates that covalent sidewall -NH₂ functionalization is as effective as direct substitutional doping in lowering the IP values which are beneficial for field emission. The magnetic moment of chemisorbed N adatom ranges from 0.5 to 0.7 μ_B and depends on the nanotube chirality and diameter and the orientation of the chemisorbed N adatom as well. Our study also indicates that structural relaxation of SWNTs with two chemisorbed N adatoms in certain perpendicular configurations may result in the formation of N-N bond, mainly due to the breaking or elongating of the bridged C-C bonds. The coalescence of two neighboring N adatoms into a N₂ molecule needs to overcome an energy barrier in the range between 0.9 and 3.4 eV, depending on the N-chemisorption configuration and tubular diameter.

*Author to whom correspondence should be addressed. lin_jianyi@ices.a-star.edu.sg

¹T. W. Odom, J. Huang, P. Kim, and C. M. Lieber, *Science* **391**, 62 (1998).

²R. S. Lee, H. J. Kim, J. E. Fischer, A. Thess, and R. E. Smalley, *Nature (London)* **388**, 255 (1997).

³K. Suenage, M. P. Johansson, N. Hellgren, E. Broitman, L. R. Wallenberg, C. Colliex, J. Sundgren, and L. Hultman, *Chem. Phys. Lett.* **300**, 695 (1999).

⁴S. H. Lim, H. I. Elim, X. Y. Gao, A. T. S. Wee, W. Ji, J. Y. Lee, and J. Lin, *Phys. Rev. B* **73**, 045402 (2006).

⁵R. Droppa, Jr., C. T. M. Ribeiro, A. R. Zanatta, M. C. dos Santos, and F. Alvarez, *Phys. Rev. B* **69**, 045405 (2004).

⁶F. Villalpando-Paez, A. Zamudio, A. L. Elias, H. Son, E. B. Barros, S. G. Chou, Y. A. Kim, H. Muramatsu, T. Hayashi, J. Kong, H. Terrones, G. Dresselhaus, M. Endo, M. Terrones, and M. S. Dresselhaus, *Chem. Phys. Lett.* **424**, 345 (2006).

⁷B. N. Khare, P. Wilhite, R. C. Quinn, B. Chen, R. H. Schingler, B.

- Tran, H. Imanaka, C. R. So, C. W. Bauschlicher, Jr., and M. Meyyappan, *J. Phys. Chem. B* **108**, 8166 (2004).
- ⁸B. Khare, P. Wilhite, B. Tran, E. Teixeira, K. Fresquez, D. N. Mvondo, C. Bauschlicher, Jr., and M. Meyyappan, *J. Phys. Chem. B* **109**, 23466 (2005).
- ⁹Z. Konya, I. Vesselenyi, K. Niesz, A. Kukovecz, A. Demortier, A. Fonseca, J. Delhalle, Z. Mekhalif, J. B. Nagy, A. A. Koos, Z. Osvath, A. Kocsonya, L. P. Biro, and I. Kiricsi, *Chem. Phys. Lett.* **360**, 429 (2002).
- ¹⁰J. Kotakoski, A. V. Krasheninnikov, Y. Ma, A. S. Foster, K. Nordlund, and R. M. Nieminen, *Phys. Rev. B* **71**, 205408 (2005).
- ¹¹I. Hagiri, N. Takahashi, and K. Takeda, *J. Phys. Chem. A* **108**, 2290 (2004).
- ¹²Y. Ma, A. S. Foster, A. V. Krasheninnikov, and R. M. Nieminen, *Phys. Rev. B* **72**, 205416 (2005).
- ¹³B. Delley, *J. Chem. Phys.* **92**, 508 (1990).
- ¹⁴J. P. Perdew, K. Burke, and M. Ernzerhof, *Phys. Rev. Lett.* **77**, 3865 (1996).
- ¹⁵B. Delley, *Int. J. Quantum Chem.* **69**, 423 (1998).
- ¹⁶H. J. Monkhorst and J. D. Pack, *Phys. Rev. B* **13**, 5188 (1976).
- ¹⁷R. Czerw, M. Terrones, J.-C. Charlier, X. Blasé, B. Foley, R. Kamalakaran, N. Grobert, H. Terrones, D. Tekleab, P. M. Ajayan, W. Blau, M. Ruhle, and D. L. Carroll, *Nano Lett.* **1**, 457 (2001).
- ¹⁸N. Govind, M. Petersen, G. Fitzgerald, D. King-Smith, and J. Andzelm, *Comput. Mater. Sci.* **28**, 250 (2003).
- ¹⁹C. Sun, H. Wang, M. Hayashi, L. Chen, and K. Chen, *J. Am. Chem. Soc.* **128**, 8368 (2006).
- ²⁰H. C. Choi, S. Y. Bae, J. Park, K. Seo, C. Kim, B. Kim, H. J. Song, and H. J. Shin, *Appl. Phys. Lett.* **85**, 5742 (2004).
- ²¹M. Terrones, R. Kamalakaran, T. Seeger, and M. Ruhle, *Chem. Commun. (Cambridge)* **2000**, 2335 (2000).
- ²²H. Pan, Y. P. Feng, and J. Y. Lin, *Phys. Rev. B* **70**, 245425 (2004).
- ²³J. Zhao, H. Park, J. Han, and J. P. Lu, *J. Phys. Chem. B* **108**, 4227 (2004).
- ²⁴K. Kong, S. Han, and J. Ihm, *Phys. Rev. B* **60**, 6074 (1999).
- ²⁵H. S. Kang and S. Jeong, *Phys. Rev. B* **70**, 233411 (2004).
- ²⁶M. Zhao, Y. Xia, Y. Ma, M. Ying, X. Liu, and L. Mei, *Phys. Rev. B* **66**, 155403 (2002).
- ²⁷A. Maita, J. Andzelm, N. Tanpipat, and P. von Allmen, *Phys. Rev. Lett.* **87**, 155502 (2001).
- ²⁸H. S. Kang, *J. Phys. Chem. B* **110**, 4624 (2006).
- ²⁹H. F. Bettinger, T. Dumitrica, G. E. Scuseria, and B. I. Yakobson, *Phys. Rev. B* **65**, 041406 (2002).